Published on:

International Journal of Hydrogen Energy 36 (2011) 15783-15793

doi:10.1016/j.ijhydene.2011.08.102

PREPARATION, TESTING AND MODELLING OF A HYDROGEN SELECTIVE Pd/YSZ/SS COMPOSITE MEMBRANE

R.Sanz[1], J.A. Calles[1], D. Alique[1], L. Furones[1], S. Ordóñez[2], P.Marín[2], P. Corengia[3], E. Fernández[3]

[1] Department of Chemical and Energy Technology, Rey Juan Carlos University C/ Tulipán s/n, 28933 Móstoles, Madrid, SPAIN

[2] Department of Chemical Engineering and Environmental Technology, University of Oviedo, Facultad de Química, C/Julián Clavería 8, 33006 Oviedo, SPAIN

[3] *Tecnalia, Mikaletegi Pasealekua 2, 20009 San Sebastián, Donostia,* SPAIN

ABSTRACT

A palladium selective tubular membrane has been prepared to separate and purify hydrogen. The membrane consists of a composite material, formed by different layers: a stainless steel support (thickness of 1.9 mm), an yttria-stabilized zirconia interphase (thickness of 50 μm) prepared by Atmospheric Plasma Spraying and a palladium layer (thickness of 27.7 μm) prepared by Electroless Plating. The permeation properties of the membrane have been tested at different operating conditions: retentate pressure (1 – 5 bar), temperature (350 – 450ºC) and hydrogen molar fraction of feed gas (0.7 – 1). At 400ºC, a permeability of $1.1 \cdot 10^{-8}$ mol/(s m $Pa^{0.5}$) and a complete selectivity to hydrogen were obtained. The complete retention of nitrogen was maintained for all tested experiment conditions, with both single and mixtures of gases, ensuring 100% purity in the hydrogen permeate flux.

A rigorous model considering all the resistances involved in the hydrogen transport has been applied for evaluating the relative importance of the different resistances, concluding that the transport through the palladium layer is the controlling one. In the same way, a model considering the axial variations of hydrogen concentration because of the cylindrical geometry of the experimental device has been applied to the fitting of the experimental data. The best fitting results have been obtained considering Sieverts'-law dependences of the permeation on the hydrogen partial pressure.

Keywords: Hydrogen separation, palladium composite membrane, Electroless plating, permeation model.

1. INTRODUCTION

The present energy system based on fossil fuels is clearly unsustainable because it will not be able to provide continuous economic growth and contribute to the environmental protection. Hydrogen could be a promising energy vector because its versatility and efficiency (especially in fuel cell devices) [1]. However, the development of economic and environmentally sustainable hydrogen production technologies is a key factor for implementing completely the hydrogen economy. Nowadays, about 96% of hydrogen is obtained from fossil fuels, producing a mixture of carbon monoxide and hydrogen that is so-called syngas and it cannot be used directly in final applications such as fuel cell systems [2]. This syngas can be subsequently converted into CO_2-H_2 mixtures by using Water Gas Shift Reaction (WGSR) and/or Preferential CO Oxidation (PROX). An effective separation of the hydrogen from the carbon oxides will enable carbon capture and sequestration procedures, leading to hydrogen with zero net carbon emissions. Among the different alternatives being under investigation, membrane technology is a very promising challenge because of its low energy requirements and the absence of auxiliary chemicals. It is fully accepted that palladium is the most efficient phase for selective hydrogen permeation, composite palladium membranes being proposed in order to join high permeation selectivity with lower membrane costs, especially if compared with dense Pd membranes [3-4].

Therefore, proposed palladium membranes are usually configured as a multilayer system, being supported on porous stainless steel (PSS) or alumina for minimizing the Pd thickness and consequently, the cost of the membrane [3]. In these configurations, the selection of the material for each layer is crucial since differences in the thermal expansion coefficient of each one might provoke the generation of shear stresses and crack formation. Moreover, it is important to emphasize that the expansion and contraction of palladium layer with temperature is strongly influenced by the hydrogen sorption or desorption, being possible changes in the metal lattice up to 5 times. Despite this, the similar thermal expansion coefficient of stainless steel and palladium makes this alternative very attractive, increasing the stability of the composite membrane during the consecutive heating and cooling cycles of the hydrogen separation processes as compared with other supports [4]. However, PSS supports present larger roughness and average pore size than ceramic ones [5] and these systems often include an intermediate layer for improving the surface properties and preventing intermetallic diffusion from the PSS support to the Pd layer [6]. A wide variety of materials have been proposed as intermediate layer such as silica [7], alumina [8], aluminium hydroxide [9], zeolites [10-11], ceria [12] or zirconia [13-15]. It is clear that properties of the

barrier are of crucial importance for the performance of the final membrane, mainly attending to the economy, porosity, adherence and thermal stability of the composite system. Among all of mentioned materials, the last one, zirconia, offers a thermal expansion coefficient very close to both PSS and palladium, maintaining reasonable properties related to adherence and economy [13]. Several techniques are available to deposit the palladium selective layer although the most widely used preparation method is the electroless plating (ELP) due to their ability for covering supports with complex geometries, the simplicity of the required equipment and its low cost (absence of electrodes or electrical source) [16]. This technique is based on the controlled autocatalytic reduction of metallic complexes, usually $Pd(NH_3)_4Cl_2$, on the target surface in the presence of a reducing agent, typically hydrazine [17].

In the present work, experimental tests are presented for determining and modelling the permeation properties of a Pd composite membrane prepared by electroless plating over a porous stainless steel support with yttrium- stabilized zirconium oxide (YSZ) as intermediate layer. The palladium layer is prepared to be thick enough to avoid pin-holes and to ensure good hydrogen selectivity. Permeation behaviour will be modelled using a theoretical model that accounts for the different mass transfer resistances of the membrane layer: porous layers are modelled using the dusty-gas-model, whereas for the palladium dense layer the Sieverts' law is used. Modelling approach used in the present work accounts for the axial variations of the hydrogen concentration because of the permeation, these variations being important in tubular devices as the used in this work. By contrast, most of the modelling approaches reported in the literature consider total mixing of the gases in each side of the membrane and works with averaged values of the hydrogen concentration [18].

The model parameters are determined from membrane characterization data and fitting of the experimental permeation data. This model can be used to predict permeation properties of similar membranes, as well as for the design of membrane reactors for accomplishing methane reforming or WGS reactions with simultaneous hydrogen separation. In this way, chemical equilibrium will be favourably shifted in addition to get high purity hydrogen.

2. METHODOLOGY

2.1. Membrane preparation

Tubular stainless steel supports (PSS) with a porosity of ca. 20% and media grade of 0.1 μm (which means that 95% rejection of particles with a size greater than the grade is guaranteed) were provided by Mott Metallurgical. The supports have a thickness of 1.9 mm, external diameter of 12.9 mm and a length of 610 mm. PSS pieces of 70 mm length were obtained by cutting the original ones and dense stainless steel tubes were welded on both extremes for ensuring the sealing in the permeation experiments. In this process, the effective porous area of the support was reduced until an equivalent length of 62 mm.

Before further treatment of the commercial supports, they were cleaned in order to remove surface pollutants, such as oil, grease or dust. The process consisted of consecutive immersions in solutions of sodium hydroxide 0.1 M for 5 min, hydrochloric acid 0.1 M for 5 min and pure ethanol for 15 min. All washing steps were performed at 65ºC under ultrasonication stirring. After each washing step, supports were rinsed with distilled water. The process is completed with a drying step by air at 110 °C for 8 hours.

Once the PSS supports have been cleaned, an YSZ intermediate layer was incorporated. The deposition was carried out by atmospheric plasma spraying (APS) technique using a APS F4 equipment (Sulzer-Metco). The PSS support was placed on a lathe turning around its own axis (at 200 rpm). YSZ powder (AMDRY 6660; ZrO_2-$20Y_2O_3$) was fed to the equipment, semi-fused and then deposited by a spray gun, obtaining a homogeneous coating. The APS process conditions were: 630 A DC, 40 L/min of argon, 12 L/min hydrogen, and 4 L/min of carrier gas. The thickness for each coating was controlled by counting the turns of the support while the powder was deposited on it. After the coating deposition, the obtained layer was sand-blasted in order to decrease its surface roughness.

The development of a selective Pd layer over the intermediate layer of YSZ was carried out by Electroless Plating (ELP). This process involves two different steps: the surface activation and the metal deposition. The surface activation of PSS modified with an intermediate layer is necessary in order to initiate a homogeneous plating process with a relative low induction period. This first step involves successive dips of the support in an acidic solution of palladium (0.1 g/L) and a solution of hydrazine-ammonia (Table 1). Gentle rinsing with deionized water after each immersion bath was carried out for preventing the contamination of solutions employed. These immersions were performed at room temperature with a controlled vertical rotation of PSS support (50 rpm) to ensure suitable activation homogeneity over the whole PSS piece. Moreover, the ends of the supports were covered with Teflon tapes to avoid the solution to come into the internal surface of PSS sample. The activation was repeated 6 times

in order to achieve an homogeneous distribution of Pd nuclei. In the second step of the ELP process, Pd deposition, the activated supports were immersed into a plating solution under vertical rotation at 50 ºC. The detailed composition of the plating bath and the deposition conditions are also given in Table 1. In this step, the palladium deposition was produced by adding, in several doses, the reducing agent (N_2H_4) to the plating solution. The latter contains the metallic source ($PdCl_2$), the complexing agent (NH_4OH) and the stabilizer (EDTA). Finally, membranes were gentle rinsed with deionized water and dried at 110 ºC for 8 hours. The Pd thickness for each membrane was controlled by using different number of immersions in the plating solution.

2.2. Membrane characterization

The morphology of prepared composite membranes were analysed by Scanning Electron Microscopy (Philips XL30 SEM) equipped with an Energy Dispersive Analytical System (EDAS) for microprobe analysis. Moreover, SEM images were processed with two specific software packages used in electron microscopy. Digital Micrograph TM (Gatan) was used for calculation the pore size distribution on the surface from the backscattering electron (BSE) images obtained by SEM. Scanning Probe Image Processor (SPIP®, Image Metrology) was used to determine the surface roughness from gas scattering electron (GSE) SEM images.

Moreover, several parameters related to the membrane physical properties such as porosity, mean pore size or tortuosity were determined by Mercury Intrusion Porosimetry (AutoPre IV 9500 V1.09 91-473-01). In order to analyze each sample, 0.15-0.20 g were introduced in a 5 mL sample cup containing the mercury and the pressure was accurately increased from 0.07 to 2.27 barg.

The average intermediate YSZ layer thickness was measured by Scanning Electron Microscopy (Philips XL30 SEM) while the Pd layer thickness was estimated by gravimetric analysis (electronic balance Kern & Sohn ABS-4 with a precision of ±0.0001 g) from the data of the weight gained just after ELP step.

2.3. Permeation experiments

Permeation experiments were performed in a home-made equipment (Figure 1) to determine the permeability and the separation factor of the membrane. Different gases were available to

test individual feed gas (nitrogen and hydrogen) and prepare feed gas mixtures (nitrogen-hydrogen mixtures). Permeation measurements were performed in the range of 0.3-4.0 bar (in the retentate side) at temperatures upper to 300ºC (experiments in the range 350-450ºC) to avoid the Pd layer embrittlement due to the coexistence of α-β hydrogen-palladium hybrids in the composite membranes prepared. The permeation system basically consisted of a 316L stainless steel cell that contains the palladium membrane placed between two graphite O-rings to ensure the seal between the retentate and permeate sides. Finally, two copper O-rings were used for the external sealing of the system. This assembly is placed into a furnace for achieving the desired temperature in each experiment.

2.4. Permeation model

The composite membrane prepared in this work is formed by stacked layers of different materials, as show in Figure 2, constituting a complex mass transfer media. Thus, each different layer and the gas phase boundary layers, represent potential mass transfer resistances. In palladium-based composite membranes used for hydrogen permeation, the palladium layer is usually the most important mass transfer resistance, due to the solution-diffusion mass transfer mechanism. However, depending on the operating conditions, the thickness of the different layers or the material itself, more than one mass transfer resistance may contribute to the overall mass transfer [19-21]. Caravella et al. [20] developed a detailed mass transfer model for a palladium composite membrane and studied the influence of the operating conditions and palladium layer thickness on the mass transfer resistances. They found that, for a palladium thickness of 10 μm, the controlling resistance is the hydrogen bulk diffusion in the palladium, whereas for a thickness of 1 μm, the mass transfer in the porous support may also be important.

At this point, four potential mass transfer resistances have been identified, as shown in Figure 2: gas phase at the retentate side, porous support layer (PSS), porous interphase layer (YSZ), and the palladium selective layer. It should be taken into account that when hydrogen selectivity is 100% and no sweep gas is used in the permeate side, as in the present work, gas phase mass transfer resistance at the permeate side is zero. Mass transfer in the gas phase and the support and interphase layers are well known, so they can be predicted using correlations from the literature [20, 22-23]. These correlations have been re-written as the resistance form:

$$J_{H_2} = \frac{\Delta_j p_{H_2}}{R_j} \quad (1)$$

Where R_j is the *j*-mass transfer resistance, shown in Table 2, and $D_j p_{H_2}$ is the hydrogen partial pressure gradient for the *j*-mass transfer resistance.

Gas phase resistance at the retentate side is calculated using the boundary layer theory for unidirectional and high concentration mass transfer [20]. The binary diffusion coefficient for hydrogen and nitrogen mixtures has been determined using the Fuller equation [24]:

$$D_{H_2,N_2} = \frac{0.0143\ T^{1.75}}{p_r M_{H_2,N_2}^{0.5}\left[\left(\sum \upsilon_{H_2}\right)^{2/3} + \left(\sum \upsilon_{N_2}\right)^{2/3}\right]} \quad (2)$$

Where $M_{H_2,N_2}=2/(1/M_{H_2}+1/M_{N_2})$, and $E\upsilon_{H_2}$= 6.12 and $E\upsilon_{N_2}$=18.5 are the sum of the atomic volumes for hydrogen and nitrogen, respectively.

The porous support and interphase layers are both modelled using the dusty-gas model, which accounts for viscous and Knudsen flow in porous media [22-23]. Hydrogen effective Knudsen diffusion coefficient is calculated using the following expression [25], where the porosity (ε), tortuosity (τ) and pore size (d_p) corresponding to each layer, determined by mercury intrusion porosimetry, are used. The geometrical and physical properties of the different layers are summarized in Table 3.

$$D_{\varepsilon K} = \frac{2}{3}\frac{\varepsilon}{\tau} d_p \sqrt{\frac{2\,R\,T}{\pi\,M_{H_2}}} \quad (3)$$

Hydrogen viscosity has been determined using an empirical temperature-dependent expression [25]:

$$\mu_{H_2} = \frac{1.797\cdot 10^{-7}\ T^{0.685}}{\left(1-\frac{0.59}{T}+\frac{140}{T^2}\right)} \quad (4)$$

Hydrogen mass transfer inside the palladium layer exhibits a complex mechanism formed by different steps in series, as described by different authors [20-21]: adsorption, surface to bulk transport, bulk diffusion, bulk to surface transport and desorption. At the operating conditions

and the membranes used in hydrogen permeation, these steps can be modelled using Sieverts' law, with exponent *n* equal to 0.5:

$$J_{H_2} = \left(\frac{Q}{\delta_{Pd}} \right) \left(p_{H_2 r}^{n} - p_{H_2 p}^{n} \right) \tag{5}$$

Where $Q=Q_0 \exp(-E_a/RT)$ is the permeability of the membrane, which commonly follows Arrhenius-type dependence with temperature. The permeability and the activation energy cannot be predicted and must be determined experimentally for the actual membrane.

The Richardson's law is a generalization of Sieverts' law with an exponent *n* different from 0.5. The use of this expression to model the overall mass transport is very common, even if there are important mass transfer resistances different from the palladium layer [26]. In this case, the exponent *n* that best fits the experimental data [27] is used. Thus, it has been reported exponent values different from 0.5 for thin palladium layers, when the hydrogen bulk diffusion in the palladium is not the controlling step [28], or the crystallographic structure of the layer is not homogeneous, i.e. due to dislocations, crystal fractures, etc. [29].

2.5. Membrane model

In plate-type membranes, the flux predicted by permeation equations (1) and (5) is the same for the whole membrane surface, because both retentate and permeate hydrogen partial pressure are uniform. On the contrary, in tubular membranes, hydrogen concentration decreases on the retentate side from the inlet to the outlet, and hence the flux also decreases [30]. In order to model this behaviour accurately, the differential mass balances to the retentate side must be formulated:

$$\frac{dF_{H_2 r}}{dA_m} = -J_{H_2} \qquad , \qquad F_{H_2 r}\Big|_{A_m=0} = y_{H_2 f} F_f \tag{6}$$

Where, as hydrogen concentration, the hydrogen flux J_{H_2} varies from the inlet to the outlet of the membrane tube; the corresponding value is evaluated using a suitable permeation model (equations (1) and (5)). The mean hydrogen flux can be easily calculated using the following expression, where it has been considered that on the permeate side hydrogen molar fraction is 1.

$$\left\langle J_{H_2} \right\rangle = \left(y_{H_2 f} F_f - F_{H_2 r}^{out} \right) / A_m \tag{7}$$

The previous model has been solved using a MATLAB code that performs all the calculations; `ode15s` function is used to solve the ordinary differential equation.

This model has also been used to determine the unknown parameters of the permeation model, mainly permeability and activation energy, by fitting the experimental mean hydrogen flux using the least-square method. In each step of the solving procedure, the previous model is evaluated for the whole set of experiments and the simulated mean hydrogen flux is compared to the experimental one. The calculations are done using a MATLAB code that uses `patternsearch` function first to find an initial guess of the fitting parameters, and then `lsqcurvefit` function is executed with this initial guess.

3. RESULTS AND DISCUSSION

3.1. Membrane morphology

The composite membrane prepared in this work is formed by adding an inorganic intermediate layer of yttria-stabilized zirconia (YSZ) over the raw PSS support and incorporating the Pd selective layer by electroless plating technique (ELP). Figure 3 shows the SEM images of raw support and the surface obtained just after each incorporated layer (YSZ and selective Pd layers). As it can be seen, commercial PSS support is formed by agglomeration of heterogeneous particles of stainless steel with sizes in the range of 1-20 μm. The surface presents a non-uniform pore size distribution with presence of larges pores, greater than specified grade (0.1 μm) (Figure 3a). Analysing this SEM image with both Digital Micrograph and Scanning Probe Image Processor software, a porosity about 20% and an average roughness value of S_a=6.25 μm were obtained. The image of the support modified by incorporation of an YSZ intermediate layer is shown in Figure 3b. This intermediate layer maintains a similar morphology to that of the original support, in spite of the incorporated thickness, 50 μm. Analysing the surface in detail with both digital software tools mentioned above, it can be seen that the presence of large pore mouths on the surface was considerably reduced (porosity of 1.96 %) although a relatively high roughness was still maintained (S_a=4.73 μm). In this manner, it seems evident that the surface modification of the raw PSS support is produced after the incorporation of the YSZ intermediate layer. Finally, the SEM image of the composite membrane obtained after the Pd incorporation by ELP is shown in Figure 3c. In this

case, the palladium covers most of the modified support surface with low Pd thickness (around 5-6 μm), but the irregularities on the surface (mainly the high roughness) provoke the presence of pinholes that only can be covered by increasing the Pd thickness up to 27.7 μm. Eventually, the obtained composite PSS-YSZ-Pd membrane presents a negligible porosity (around 0.2 %) and a roughness of S_a= 3.37 μm that is maintained after permeation tests.

In the last few years, much effort has been devoted to the development and optimization of economic routes for preparing membranes with high selectivity. The major aim of the studies presented in the literature is the reduction of the palladium thickness, decreasing both material and operating costs, without compromising the thermal and mechanical integrity of the membrane. In this context, it is possible to find a wide variety of thickness in the composite palladium membranes presented in the literature according to their specific application. In this manner, although the general trend is to obtain a Pd thickness below 10 μm [31], recent works also present membranes with thickness considerably higher for ensuring a good selectivity and suitable mechanical resistance [32-33]. It is important to emphasize that the reduction of thickness usually limits the theoretically complete selectivity of the membrane [4] due to the presence of defects and pinholes. Summarizing, it is possible to conclude that the PSS/YSZ/Pd composite membrane presented in this work is a representative case of the current membrane preparation status and really useful for developing theoretical permeation models that can be extended to any current Pd membrane.

3.2. Experimental permeation behaviour

In order to study the permeation properties of the composite membrane, a set of single gas permeation experiments with both pure nitrogen and hydrogen have been carried out at 400ºC. From these experiments, the permeability and the ideal separation factor (calculated as the ratio between hydrogen and nitrogen fluxes) of the prepared membrane have been determined. At this point, it was found that the membrane is completely impermeable to nitrogen since nitrogen flux was not detected in the permeate side. Therefore, it is concluded that the Pd layer was totally selective to H_2, obtaining a permeance of $4.05 \cdot 10^{-4}$ mol/m^2·s·Pa$^{0.5}$.

A complete comparison of the obtained results with data recently reported in the literature from some different palladium composite membranes is shown in Table 4. Several parameters are reported in the table: membrane type, preparation method, thickness of the Pd selective layer, and experimental conditions of the permeation experiments (temperature and pressure

ranges), hydrogen flux, hydrogen permeance, ideal selectivity and the reference of the work. So as it can be seen, in most cases, the permeation properties of each membrane are intimately related to their thickness. The thinnest membranes present higher hydrogen fluxes and permeances. However, the probability of presence of Pd defects and pinholes is greater and the ideal selectivity decreases, in contrast with thicker membranes that present lower values of permeance but the selectivity trends to infinite. The membrane presented in this work shows a hydrogen permeance lightly lower than other membranes, although an infinite selectivity to hydrogen is achieved.

Permeation experiments with both nitrogen and hydrogen gases were repeated in order to determine the stability of the membrane under operation conditions (single gases at 400ºC). Thus, five consecutive cycles of heating and cooling were performed at four different hydrogen partial pressures (0.5, 0.8, 1.0 and 1.2 bar), measuring the permeation properties at the end of each cycle. Figure 4 shows the permeation measurements obtained in these experiments. Each of the hydrogen flux data that is shown in the graph represents the average of the five cycles carried out. As it can be seen, the reproducibility of the hydrogen fluxes for each driving force (ΔP) is very high, obtaining random variation of the fluxes and errors below 5% for all cases. This fact evidences the stability of the prepared PSS-YSZ-Pd membrane to thermal cycles. In this graph, only H_2 flux is represented since N_2 was not detected experimentally in any case, indicating a complete selectivity to hydrogen. On the other hand, it can be also observed that the hydrogen flux increases linearly with $\Delta P^{0.5}$in the range of measurements. This trend is consistent with the solution-diffusion model of permeation through a palladium membrane when the rate-determining step is the diffusion of hydrogen in the free-pinhole metallic film. The generation of pin-holes after several heating and cooling cycles provokes deviations in the exponential coefficient (0.5) so the results obtained suggest a good stability of the membrane under temperature cycles.

In order to determine the influence of the hydrogen concentration in the feed gas and to develop a theoretical model for predicting the permeation properties of Pd membranes, a new set of experiments was performed with binary gas mixtures (H_2-N_2). Main operation conditions are summarised in Table 5. As in permeation experiments of pure gases, nitrogen was not detected in permeate; the chromatography analysis confirms a complete selectivity to hydrogen. Some deviation of the linear trend obtained for pure hydrogen was observed for the H_2-N_2 mixtures. Furthermore, the permeate hydrogen flux at a constant pressure difference decreases as the nitrogen content increases. The main reason for this behaviour is the reduction of the retentate hydrogen partial pressure, due to the permeation of hydrogen,

which can be modelled considering hydrogen mass balances. In addition, this behaviour maybe affected by other phenomena, such as the physisorption of nitrogen on the Pd surface, reducing the effective dissociation of hydrogen molecules, or the influence of the different mass transfer resistances. This is evaluated in the following section, devoted to the study of the mass transfer resistances involved in the permeation process. The temperature of the experiments influences lightly in the permeate flow, obtaining higher flows when the temperature increases. A detailed discussion of all these effects has been done in the modelling section, where model predictions and experimental results are compared.

3.3. Quantification of the different mass transfer resistances

In the methodology section, the permeation model was introduced, and the different potential mass transfer resistances identified. As indicated, all the resistances except one, the corresponding to the palladium layer, can be theoretically estimated using membrane geometrical and physical properties (Table 3), available from characterisation tests. In this section, the model is used to evaluate these resistances at the actual experimental conditions, so that to calculate their contribution to the experimentally determined overall mass transfer resistance. These resistances have been evaluated neglecting the influence of the tubular membrane permeation and considering uniform hydrogen concentration and equal to the mean value.

Once the individual mass transfer resistances have been evaluated, their percentage contribution to the overall resistance is calculated. This is done for each experimental permeation value, so all the information has been summarized in the form of a box plot (Figure 6). In this figure, the remaining up to 100% (not represented) corresponds to the palladium layer resistance. The most important conclusion drawn from Figure 6 is that palladium layer resistance is the most important one with more than 90% contribution in the whole set of experiments carried out. After this resistance, and on average for all the experiments, gas phase resistance is the second in importance with an average contribution of 1.5%. Nevertheless, there are a short number of experiments where support and interphase layers resistances may contribute more than the gas phase resistance, up to 3-4% of the overall mass transfer resistance.

In this section, it has been demonstrated that for the membrane used in the present work and at the conditions of the permeation experiments, the controlling mass transfer resistance is the corresponding to the palladium layer. For this reason, in the following section a simplified

permeation model, based on equation (5) and accounting only for this mass transfer resistance, has been considered.

3.4. Modelling of the permeation experiments

In this section, the permeation experiments have been fitted and the intrinsic palladium layer permeation parameters determined. As found in the previous section, the palladium mass transfer resistance is the controlling one, so the simplified permeation model defined by equation (5) can be used. This model has been solved in conjunction with a differential membrane model that accounts for the decrease in hydrogen concentration due to permeation, as described in the methodology section.

The results of the fitting together with additional statistical information are summarized on Table 6. As shown, an exponent value of 0.5, corresponding to the Sieverts' law, has been found to best fit the experimental data, which supports the findings of the previous section about the palladium layer being the controlling mass transfer resistance. The value of the activation energy (12.6 kJ/mol) is within the range (7-30 kJ/mol) of other palladium membranes from the literature (see the comparative table of Ryi et al.[27] for more details).

The performance of the model can be evaluated in Figure 5, where model predictions are compared with the experimental data. In general, it can be said that the model perform well in predicting the experiments at different temperatures, pressures differences and hydrogen inlet concentrations. However, there are some discrepancies, mainly at the lower hydrogen concentration and at very low pressures differences. The later can be explained by the small deviation of Sieverts' law reported by Guazzone et al. [29] and taking place at low pressures (1.1-2 bara). The goodness of the fitting can also be evaluated using Figure 7. The residuals plot shows a random error distribution with a maximum absolute error of 0.01 mol/(m^2 s). The predicted vs. experimental plot shows that the most remarkable deviations are for low hydrogen flux and pressure. Anyway, the model as a whole can be used to predict the performance of the membrane.

5. CONCLUSIONS

A dense palladium composite membrane, formed by a porous stainless steel support with an yttria-stabilized zirconia as an intermediate layer (interphase), has been prepared by

electroless plating. The high roughness of the support required the incorporation of an enough thick Pd layer. In this manner, a 27.7 μm of Pd selective layer thickness was necessary in order to achieve a totally dense membrane, free of defects, cracks and pinholes. The membrane has been subjected to several heating-cooling cycles at the operation conditions (400ºC), showing a good thermal stability and reproducibility of permeation data under temperature cycles. In these conditions, a hydrogen permeance in the range of $4.56\text{-}7.33\cdot10^{-7}$ mol/s·m^2·Pa was obtained, not being detected nitrogen in the permeate side for the range 0.0-5.0 bar in the retentate side. Moreover, binary permeation tests, carried out varying retentate pressure, temperature and hydrogen retentate concentration were carried out, revealing that the main mass transfer resistance involved in the hydrogen permeation is the corresponding to the palladium layer at the operating conditions. The other mass transfer resistance contributions of support, YSZ interphase layer and gas phase were negligible. All the results have been fitted to a permeation model with satisfactory performance to predict membrane permeation within the range of the operating conditions. Since the fitted parameters are intrinsic, the model can be scaled-up to model and design palladium membrane reactors.

ACKNOWLEDGMENT

This work was financed by the Spanish Ministry for Science and Innovation (contract CIT-120000-2008-4, Applied Collaborative Research Program 2008).

LIST OF SYMBOLS

Abbreviations

APS	Atmospheric Plasma Spraying
EDAS	Energy Dispersive Analytical System
ELP	Electroless plating
GSE	Gas scattering electron
PSS	Porous stainless steel
SEM	Scanning Electron Microscopy
SS	Stainless steel
YSZ	Yttria-stabilized zirconia

SSE	Standard square error

Latin symbols

A_m	membrane external area, m^2
d_p	mean pore size, m
D_{eK}	effective Knudsen diffusion coefficient, m^2/s
D_t	internal membrane diameter, m
E_a	activation energy, J/mol
F	molar flow rate, mol/s
J	permeation flux, mol/m^2 s
L	layer thickness, m
M	molar weight, kg/mol
N	partial pressure exponent
p	pressure, Pa
Q	gas flow rate at normal conditions, NmL/min
Q	membrane permeability, mol/s m Pa^n
Q_0	Permeability pre-exponential coefficient @ 0 K, mol/s m Pa^n
R	ideal gas constant, 8.314 J/mol K
R_j	*j*-mass transfer resistance, Pa s m^2 mol^{-1}
R^2_{adj}	adjusted square regression coefficient
T	temperature, K
S_a	roughness, μm
S_h	Sherwood dimensionless number
y	molar fraction

Greek letters

δ_{Pd}	palladium thickness layer, m
ΔP	pressure gradient, Pa
ε	internal porosity
ϕ	gas phase mass transfer correction factor
μ	dynamic viscosity, kg/m s
υ	atomic volume
τ	tortuosity

Subscripts

f	feed
g	gas
i	interphase
j	individual mass transfer resistance
out	outlet stream
p	permeate
Pd	palladium
r	retentate
s	support

REFERENCES

[1] Bartels JR, Pate MB, Olson NK. An economic survey of hydrogen production from conventional and alternative energy sources. International Journal of hydrogen energy 2010;35:8371-8384.

[2] Thoen PM, Roa F, Way JD. High flux palladium-copper composite membranes for hydrogen separations. Desalination 2006:224-229.

[3] Adhikari S, Fernando S. Hydrogen membrane separation techniques. Industrial Engineering Chemical 2006;45:875-881.

[4] Paglieri SN, Way JD. Innovations in palladium membranes research. Separation and Purification Methods 2002;31:1-169.

[5] Zhang K, Gao H, Rui Z, Liu P, Li Y, Lin YS. High-Temperature stability of palladium membranes on porous metal supports with different intermediate layers. Industrial Engineering Chemical Research 2009;48:1880-1886.

[6] Nam SE, Lee KH. Hydrogen separation by Pd alloy composite membranes:introduction of diffusion barrier. Journal of Membrane Science 2001;192:177-185.

[7] Su C, Jin T, Kuraoka K, Matsumura Y, Yazawa T. Thin palladium film supported on SiO2-modified porous stainless steel for a high-hydrogen-flux membrane. Industrial Engineering Chemical Research 2005;44:3053-3058.

[8] Yepes D, Cornaglia LM, Irusta S, Lombardo EA. Different oxides used as diffusion barriers in composite hydrogen permeable membranes. Journal of Membrane Science 2006;247((1-2)):92-101.

[9] Tong J, Suda H, Haraya K, Matsumura Y. A novel method for the preparation of thin dense Pd membrane on macroporous stainless steel tube filter. Journal of Membrane Science 2005;260:10-18.

[10] Bosko ML, Ojeda F, Lombardo EA, Cornaglia LM. NaA zeolite as an effective diffusion barrier in composite Pd/PSS membranes. Journal of Membrane Science 2009;331:57-65.

[11] Mabande GTP, Ghosh S, Lai Z, Schwieger W, Tsapatsis M. Preparation of b-Oriented MFI films on porous stainless steel substrates. Industrial engineering Chemical Research 2005;44:9086-9095.

[12] Tong J, Su C, Kuraoka K, Suda H, Matsumura Y. Preparation of thin Pd membrane on CeO2-modified porous metal by a combined method of electroless plating and chemical vapor depositions. Journal of Membrane Science 2006;269:101-108.

[13] Huang Y, Dittmeyer R. Preparation and characterization of composite palladium membranes on sinter-metal supports with a ceramic barrier against intermetallic diffusion. Journal of Membrane Science 2006;282:296-310.

[14] Gao H, Lin JYS, Li Y, Zhang B. Electroless plating synthesis, characterization and permeation properties of Pd-Cu membranes supported on ZrO2 modified porous stainless steel. Journal of Membrane Science 2005;265:142-152.

[15] Wang D, Tong J, Xu H, Matsumura Y. Preparation of palladium membrane over porous stainless steel tube modified with zirconium oxide. Catalysis Today 2004;93-95:689-693.

[16] Mallory O, Hajdu JB. Electroless plating. Fundamentals and applications. Amerincan electroplaters and surface finisher society; 2002.

[17] Cheng YS, Yeung KL. Effects of electroless plating chemistry on the synthesis of palladium membranes. Journal of Membrane Science 2001;182:195-203.

[18] Yun S, Ted Oyama S. Correlations in palladium membranes for hydrogen separation: A review. Journal of Membrane Science 2011;375(1-2):28-45.

[19] Caravella A, Barbieri G, Drioli E. Theoretical study of H-2 permeation through supported Pd-based membranes. Desalination 2006;200(1-3):242-244.
[20] Caravella A, Barbieri G, Drioli E. Modelling and simulation of hydrogen permeation through supported Pd-alloy membranes with a multicomponent approach. Chemical Engineering Science 2008;63(8):2149-2160.
[21] Ward TL, Dao T. Model of hydrogen permeation behavior in palladium membranes. Journal of Membrane Science 1999;153(2):211-231.
[22] Huppmeier J, Baune M, Thoming J. Interactions between reaction kinetics in ATR-reactors and transport mechanisms in functional ceramic membranes: A simulation approach. Chemical Engineering Journal 2008;142(3):225-238.
[23] Schramm O, Seidel-Morgenstern A. Comparing porous and dense membranes for the application in membrane reactors. Chemical Engineering Science 1999;54(10):1447-1453.
[24] Poling BE, Prausnitz JM, O'Connell JP. The Properties of Gases and Liquids. 5th ed. 2004.
[25] Green DW, Perry RH. Perry's Chemical Engineers' Handbook. 8th ed. 2008.
[26] Tosti S. Overview of Pd-based membranes for producing pure hydrogen and state of art at ENEA laboratories. International Journal of Hydrogen Energy 2010;35:12650-12659.
[27] Ryi SK, Xu N, Li A, Lim cJ, GRace J.R. Electroless Pd membrane deposition on alumina modified porous Hastelloy substrate with EDTA-free bath. International Journal of Hydrogen Energy 2010;35(6):2328-2335
[28] Tong J, Suda H, Haraya K, Matsumura Y. A novel method for the preparation of thin dense Pd membrane on macroporous stainless steel tube filter. Journal of Membrane Science 2005;260:10-18.
[29] Guazzone F, Engwall EE, Ma YH. Effects of surface activity, defects and mass transfer on hydrogen permeance and n-value in composite palladium-porous stainless steel membranes. Catalysis Today 2006;118:24-31.
[30] Gallucci F, Chiaravalloti F, Tosti S, Drioli E, Basile A. The effect of mixture gas on hydrogen permeation through a palladium membrane: Experimental study and theoretical approach. International Journal of Hydrogen Energy 2007;32:1837-1845.
[31] Peinemann K, Nunes SP. Membranes for energy conversion. Wiley-VCH; 2008.
[32] Basile A, Pinacci P, Iulianelli A, Broglia M, Drago F, Liguori S, Longo T, Calabro V. Ethanol steam reforming reaction in a porous stainless steel supported palladium membrane reactor. International Journal of Hydrogen Energy 2011;36:2029-2037.
[33] Pinacci P, Broglia M, Valli C, Capannelli G, Comite A. Evaluation of the water gas shift reaction in a palladium membrane reactor. 2010;156:165-172.
[34] Shi Z, Wu S, Szpunar JA, Roshd M. An observation of palladium membrane formation on a porous stainless steel substrate by electroless deposition. Journal of Membrane Science 2006;280:705-711.
[35] Lee DW, Lee YG, Nam SE, Ihm SK, Lee KH. Study on the variation of morphology and separation behavior of the stainless steel supported membranes at high temperature. Journal of Membrane Science 2003;220:137-153.
[36] Yun S, Ko JH, Oyama ST. Ultrathin palladium membranes prepared by a novel electric field assisted activation. Journal of Membrane Science 2011;369:482-489.

LIST OF TABLES

Table 1

Components and conditions	Activation baths		Plating Pd-bath
$PdCl_2$ (g/L)	0.1	-	5.4
NH_4OH 32% (mL/L)	-	119.6	390
HCl 35% (mL/L)	1.0	-	-
Na_2EDTA (g/L)	-	-	70
N_2H_4 (mL/L)	-	10	10
Temperature (ºC)	30	30	50

* $V_{solution}/S_{plating\ area}$ (cm^3/cm^2) = 3.46

Table 2

Mass transfer resistance
Retentate gas phase*
Support (PSS)
Interphase (YSZ)

*

Table 3

Internal membrane diameter,	$9.1 \cdot 10^{-3}$ m	Direct measure
External membrane diameter	$12.9 \cdot 10^{-3}$ m	Direct measure
Length	$62 \cdot 10^{-3}$ m	Direct measure
Membrane external area,	$2.513 \cdot 10^{-3}$ m^2	Direct measure
Support layer thickness,	$1.9 \cdot 10^{-3}$ m	Direct measure
Support mean pore size,	$1.88 \cdot 10^{-6}$ m	Hg porosimetry
Support internal porosity,	0.186	Hg porosimetry
Support tortuosity,	3.78	Hg porosimetry
Interphase layer thickness,	$50 \cdot 10^{-6}$ m	SEM
Interphase mean pore size,	$0.17 \cdot 10^{-6}$ m	Hg porosimetry
Interphase internal porosity,	0.12	Hg porosimetry
Interphase tortuosity,	4	Hg porosimetry
Palladium layer thickness,	$27.7 \cdot 10^{-6}$ m	Gravimetric estimation

Table 4

Membrane type	Preparation method	Pd thickness (μm)	Experimental conditions		H_2 flux ($mol/m^2 \cdot s$)	H_2 permeance ($mol/m^2 \cdot s \cdot Pa$)	Ideal selectivity (α)	Reference
			T (ºC)	ΔP (bar)				
PSS/Fe_2O_3/Pd	ELP	25	350	0.5-1.5	0.02-0.08	-	887-698	[32]
PSS/Fe_2O_3/Pd	ELP	29	400	1.0-5.0	-	$4.2 \cdot 10^{-7}$-$3.7 \cdot 10^{-7}$	550-80	[33]
PSS/Pd	ELP	3.5	500-550	0.0-3.5	0.06-0.33	-	-	[34]
PSS/YSZ/Pd	ELP	10	350-550	0.0-0.2	0.01-0.09	-	-	[15]
PSS/Ni/SiO_2/Pd	CVD	-	450	0.2-0.7	-	$6.4 \cdot 10^{-6}$	6100	[35]
PSS/CeO_2/Pd	ELP-CVD	6-10	500	1.0	0.18-0.24	-	14-108	[12]
PSS/SiO_2/Pd	CVD-ELP	2-6	500	0.5	0.04-0.18	$2.7 \cdot 10^{-6}$	300-450	[7]
α-Al_2O_3/Pd	ELP	1	450	0.3-1.2	0.05-0.45	$4.0\text{-}5.0 \cdot 10^{-6}$	3000-9000	[36]
PSS/YSZ/Pd	ELP	27.7	350-450	0.3-4.0	0.01-0.06	$4.05 \cdot 10^{-4}$ *	∞	This work

* This value is given in $mol/m^2 \cdot s \cdot Pa^{0.5}$ accordingly to the infinite selectivity of the membrane verified in the experiments (Sieverts' law)

Table 5

Operation conditions	
Feed flow rate,	200 mL/min (NTP)
Hydrogen inlet molar fraction,	0.7 – 1
Temperature,	350 – 450 ºC
Retentate pressure,	1 – 5 bara
Permeate pressure,	1 bara
Permeate hydrogen molar fraction,	1

Table 6

	$1.1 \cdot 10^{-8}$ mol/(s m $Pa^{0.5}$)
	12.6kJ/mol
	0.50
	16 164
	0.912

* Permeability at 673 K.

SSE = standard square error.

CAPTIONS TO FIGURES

Figure 1 Scheme of the home-made permeation equipment.

Figure 2 Sketch of the tubular composite membrane, indicating the different layers.

Figure 3 SEM images of membrane surface at different stages of preparation: a) Raw PSS support (grade 0.1 μm), b) after YSZ intermediate layer and c) after Pd incorporation.

Figure 4 Hydrogen flux versus the hydrogen partial pressure for single gas permeation experiments with pure H_2, for 5 consecutive cycles of heating and cooling.

Figure 5 Performance of the permeation model (symbols: experimental; lines: model). Temperature: 350ºC (upper graph), 400ºC (middle graph), 450ºC (lower graph). Hydrogen inlet molar fraction: (o) 70%, (□) 80%, (Δ) 90%, (◊) 100%.

Figure 6 Contribution of the estimated individual mass transfer resistances to the overall one. Remaining up to 100% corresponds to the palladium layer resistance.

Figure 7 Residuals (upper graph) and predicted vs. experimental (lower graph) plots for the mean hydrogen flux in mol/(m^2 s).

Figure 1

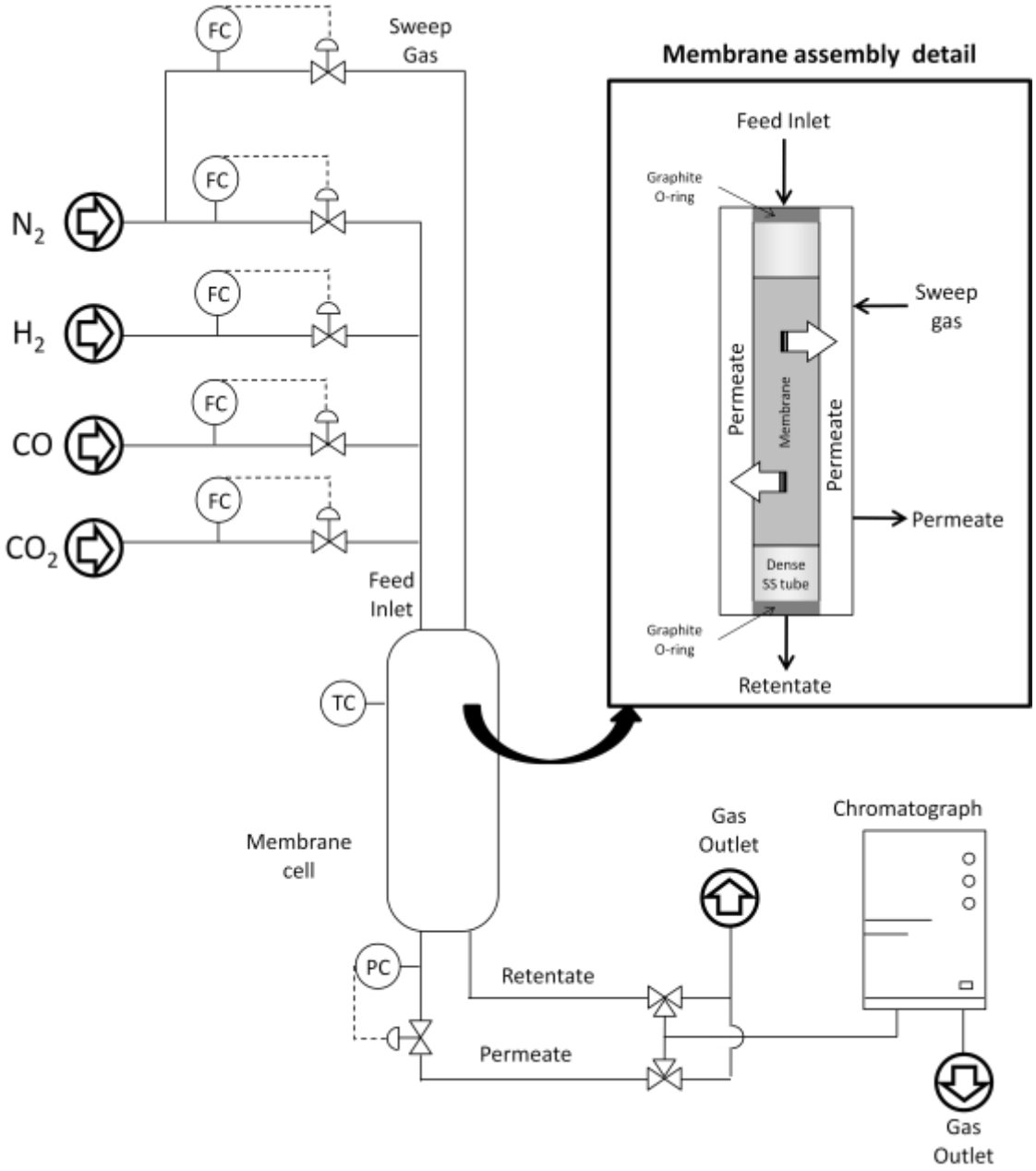
FC
Sweep Gas
FC
N_2
FC
H_2
FC
CO
FC
CO_2
Feed Inlet
TC
Membrane cell
PC
Retentate
Permeate
Gas Outlet
Chromatograph
Gas Outlet
Membrane assembly detail
Feed Inlet
Graphite O-ring
Sweep gas
Permeate
Membrane
Permeate
Permeate
Dense SS tube
Graphite O-ring
Retentate

Figure 2

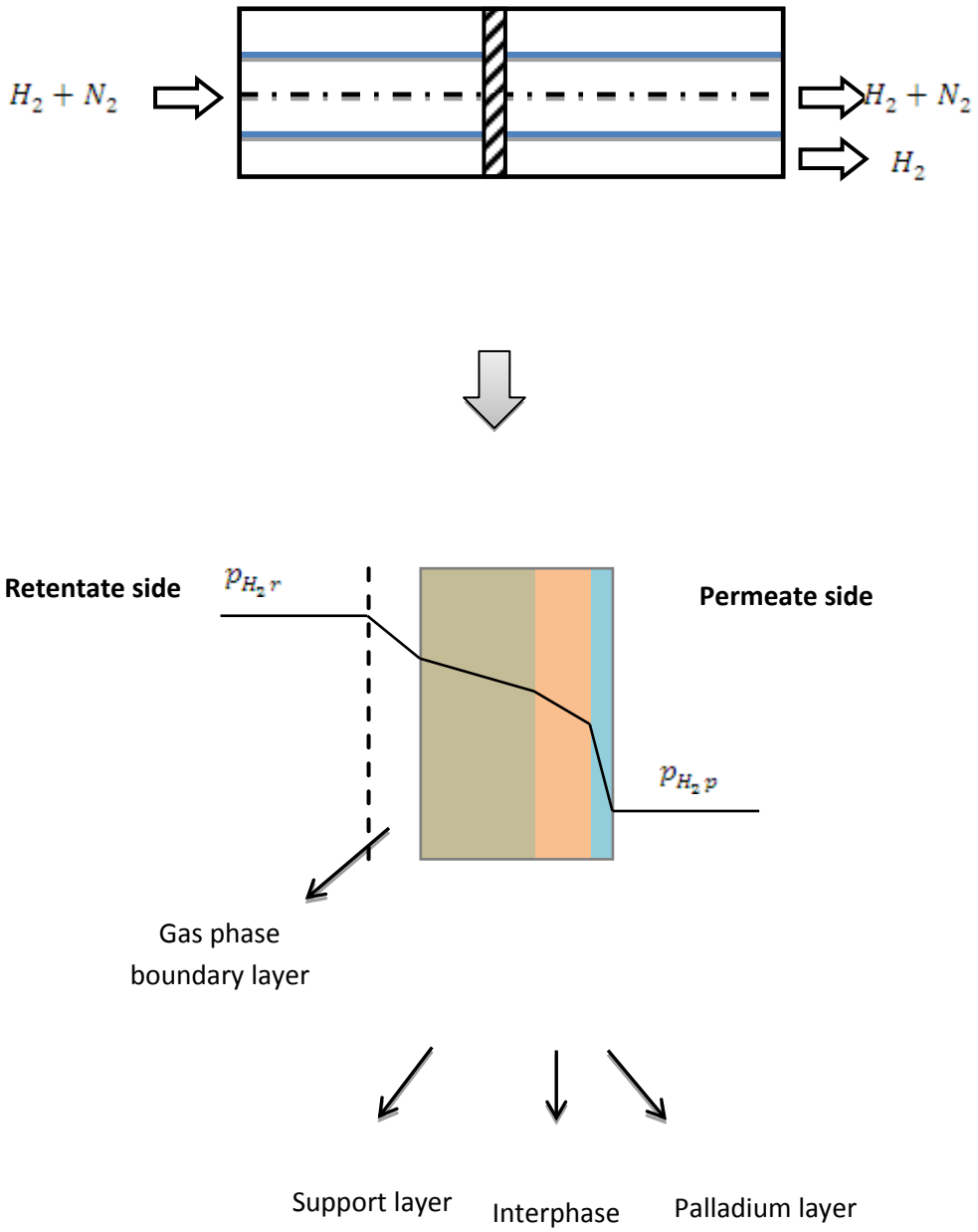
$H_2 + N_2$
$H_2 + N_2$
H_2
Retentate side
$p_{H_2 r}$
Permeate side
$p_{H_2 p}$
Gas phase
boundary layer
Support layer
(SS)
Interphase
layer (YSZ)
Palladium layer

Figure 3

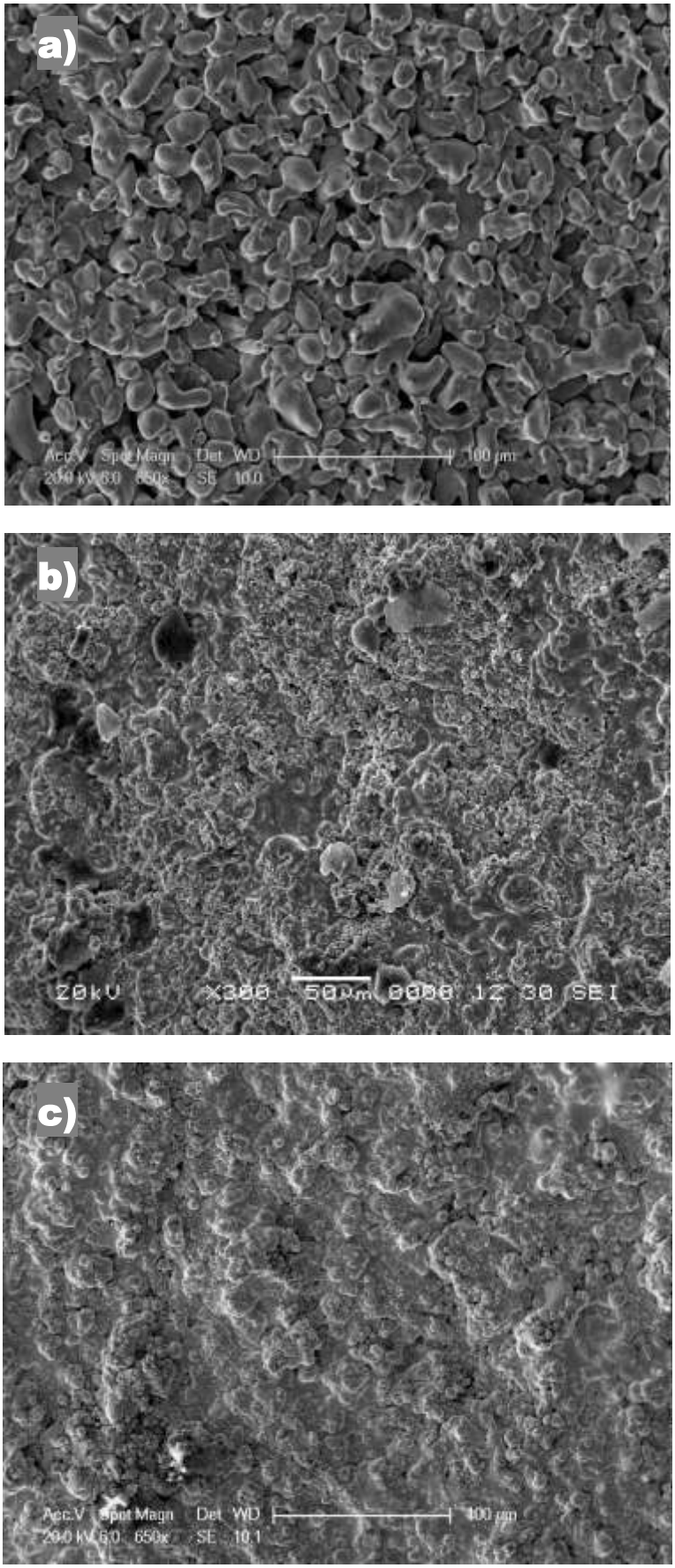

Figure 4

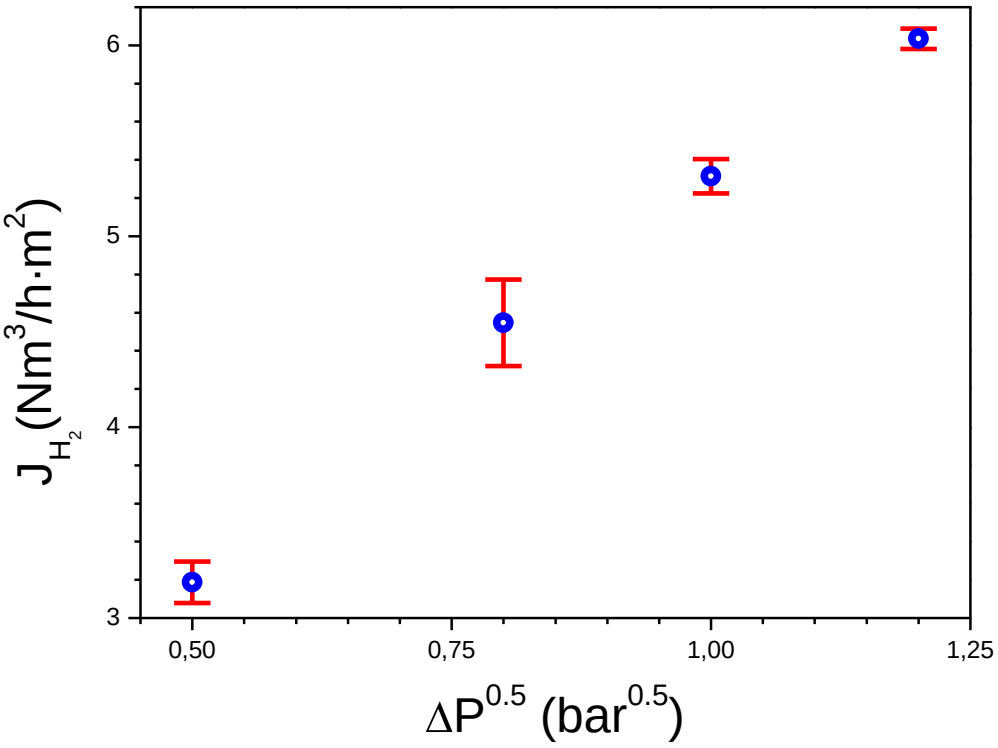

Figure 5

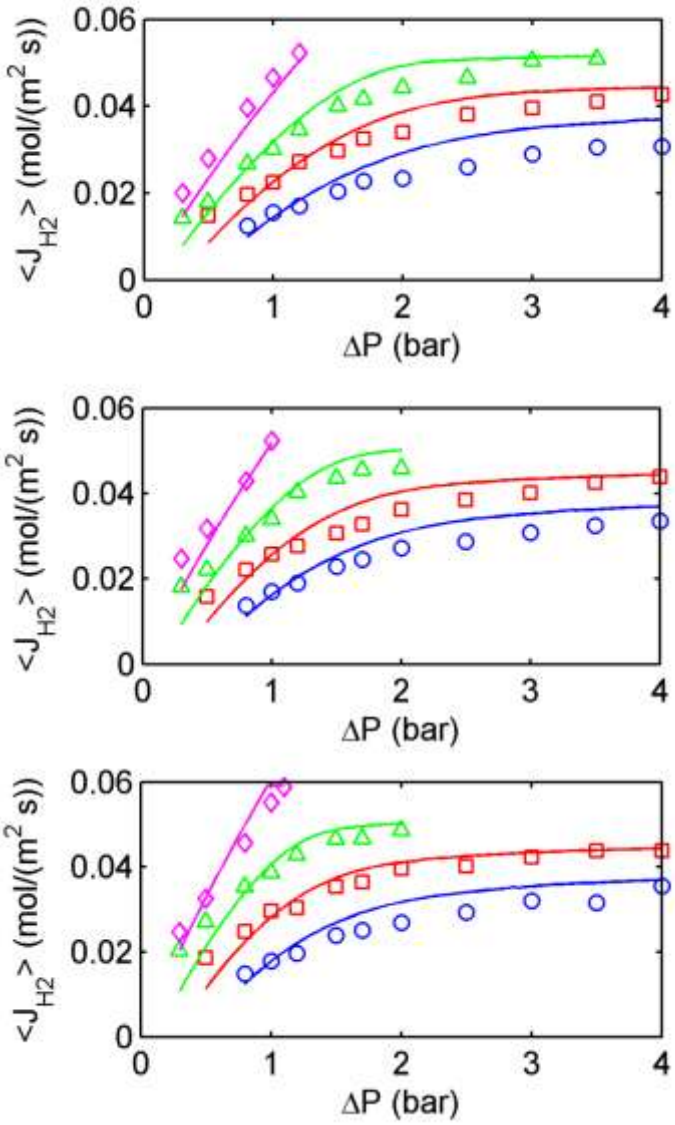

Figure 6

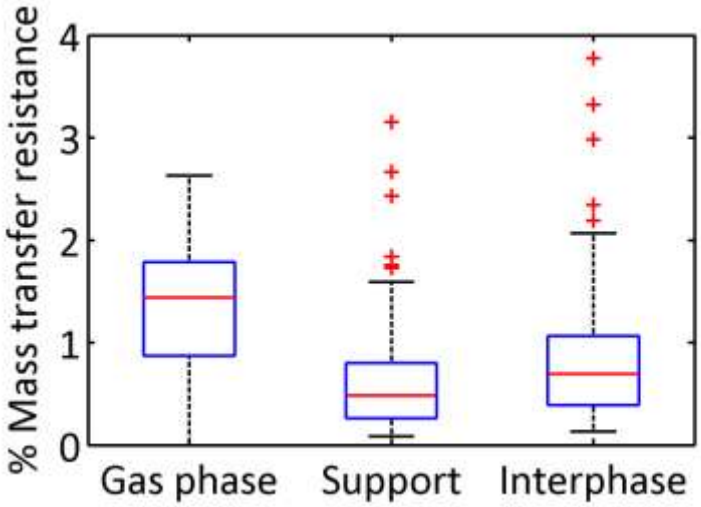
% Mass transfer resistance
0
1
2
3
4
Gas phase
Support
Interphase

Figure 7

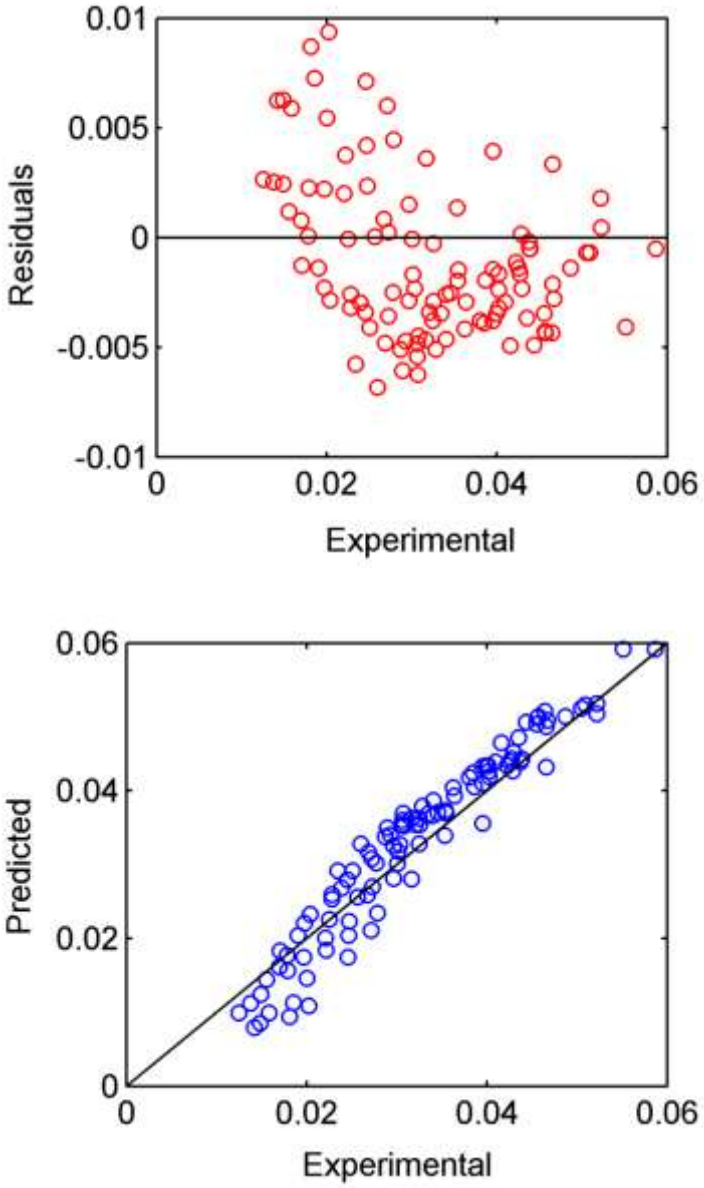
0.01
0.005
0
-0.005
-0.01
Residuals
0
0.02
0.04
0.06
Experimental
0.06
0.04
0.02
0
Predicted
0
0.02
0.04
0.06
Experimental